

# ChemComm

Chemical Communications

Accepted Manuscript

This article can be cited before page numbers have been issued, to do this please use: Z. Deng, R. Sha, H. Qin, Y. Shang, A. Yuan, W. Xie and H. Peng, *Chem. Commun.*, 2025, DOI: 10.1039/D5CC03658E.



This is an Accepted Manuscript, which has been through the Royal Society of Chemistry peer review process and has been accepted for publication.

Accepted Manuscripts are published online shortly after acceptance, before technical editing, formatting and proof reading. Using this free service, authors can make their results available to the community, in citable form, before we publish the edited article. We will replace this Accepted Manuscript with the edited and formatted Advance Article as soon as it is available.

You can find more information about Accepted Manuscripts in the [Information for Authors](#).

Please note that technical editing may introduce minor changes to the text and/or graphics, which may alter content. The journal's standard [Terms & Conditions](#) and the [Ethical guidelines](#) still apply. In no event shall the Royal Society of Chemistry be held responsible for any errors or omissions in this Accepted Manuscript or any consequences arising from the use of any information it contains.

## COMMUNICATION

## CRISPR Cas Proteins Coronated AuNP Nanostructure for Enhanced Uptake Efficiency into Cells

Received 00th January 20xx,  
Accepted 00th January 20xxZhaojia Deng <sup>a, c, ‡</sup>, Rui Sha <sup>a, ‡</sup>, Hua Qing <sup>a, b</sup>, Yingxu Shang <sup>a, c</sup>, Aijiao Yuan <sup>a, c</sup>, Wenjing Xie <sup>a, c</sup>, Hanyong Peng <sup>a, c, \*</sup>

DOI: 10.1039/x0xx00000x

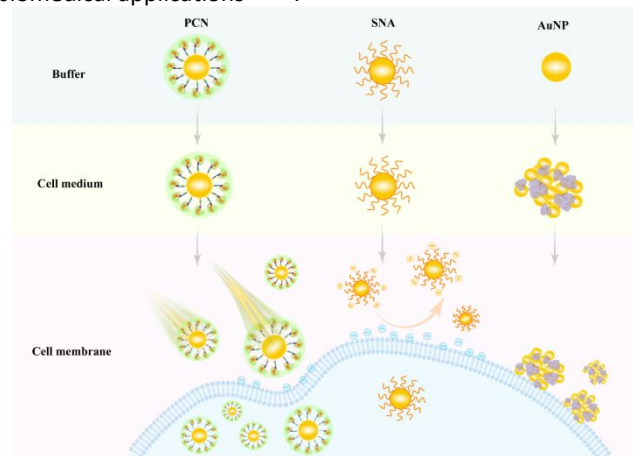
**The effectiveness of nanotechnologies is often limited by the non-specific aggregation in biological environments. We developed a proteins coronated nanostructure by functionalizing AuNPs with nucleic acid scaffolds and CRISPR Cas proteins, significantly enhancing nanoparticle stability and cellular uptake efficiency, making it a promising tool for imaging and biomedical applications.**

Nanoparticles based technologies, such as AuNPs, have emerged as versatile tools in biomedicine owing to their facile synthesis, range of sizes, biological inertness, and unique optical properties <sup>1</sup>. These properties make them promising candidates for various biomedical applications such as drug delivery, photothermal therapy, photodynamic therapy, and bioimaging. However, the effectiveness of nanoparticles is often hindered by their tendency to aggregate in complex biological environments, compromising their stability and functionality <sup>2</sup>. <sup>3</sup>. The stability and bioavailability of nanoparticles in biological media is crucial for retaining their properties and fully utilizing their biomedical potential.

The large specific surface area and high surface activity of nanoparticles can lead to aggregation, reducing their cellular delivery efficiency and increasing cytotoxicity, thus limiting their functionality in biological environments. Electrostatic repulsion is commonly employed to prevent aggregation of nanoparticles. For instance, AuNPs prepared from citrate-reduced HAuCl<sub>4</sub> possess a diffusion double layer that generates repulsive forces among the particles at low ionic concentrations, with citrate acting as both a reducing agent and a stabilizer <sup>4</sup>. However, stabilization via electrostatic repulsion <sup>5</sup>, as seen in citrate/cetyltrimethylammonium bromide (CTAB)-modified AuNPs, is susceptible to pH, salt concentration, and metal ions

in solution, posing challenges for biological applications <sup>6</sup>. Another approach involves modifying nanoparticles with polymers like poly (ethylene glycol) (PEG) to prevent particle agglomeration <sup>7, 8</sup>. While this method can enhance stability, it may increase immunogenic activity and potentially cause acute injuries to organs <sup>9, 10</sup>.

Furthermore, the introduction of nanoparticles into biological fluids results in the adsorption of proteins and small molecules onto their surface, forming unpredictable and nonspecific protein coronas. These coronas can mask the original functions of nanoparticles and alter their biological fate <sup>11, 12</sup>. The dynamic and competitive nature of protein coronas in biological fluids makes their formation unpredictable and uncontrolled, diminishing the efficacy of nanoparticles in biomedical applications <sup>13, 14</sup>.



**Scheme 1** Schematic diagram of behavior of gold nanoparticles (AuNP), spherical nucleic acids (SNA) and protein corona nanostructure (PCN) during incubation with cells.

To address these challenges <sup>15, 16</sup>, an artificial protein corona nanostructure (PCN) has been developed to enhance intracellular delivery of AuNPs (Scheme 1). This study used thiol-modified DNA strands complementary to a DNA linker, capable of hybridizing with single-guide RNA (sgRNA), to functionalize the AuNPs, followed by the binding of clustered regularly interspaced short palindromic repeats (CRISPR) associated protein (Cas9) to sgRNA to form a controlled protein corona nanostructure on the nanoparticle surface <sup>17</sup>. The study assessed the stability of these PCNs under diverse biological

<sup>a</sup> State Key Laboratory of Environmental Chemistry and Ecotoxicology, Research Center for Eco-Environmental Sciences, Chinese Academy of Sciences, Beijing, 100085, China.

<sup>b</sup> College of Science, Northeastern University, Shenyang 110819, China.

<sup>c</sup> University of Chinese Academy of Sciences, Beijing 100049, China.

<sup>‡</sup> These authors contributed equally.

\* Corresponding author

† Electronic supplementary Information (ESI) available: [details of any supplementary information available should be included here]. See DOI: 10.1039/x0xx00000x



conditions, while also studying their uptake efficiency and mechanisms. The biocompatible PCN-based delivery platform not only mitigates non-specific aggregation but also enhances cellular uptake efficiency, positioning it as a promising strategy for imaging and biomedical applications.

To synthesize the self-assembled protein coronated nanostructure (PCN), the initial step involved modifying the surface of gold nanoparticles with a nucleic acid inner layer. This process entailed connecting the sgRNA to a thiol-modified anchor strand via a linker strand, resulting in the formation of a three-strand complex. By anchoring this nucleic acid complex to the surface of 20 nm gold nanoparticles through Au-S bonds facilitated by the thiol group at the 5' end of the anchor strand, a nucleic acid inner layer was established, leading to the creation of a spherical nucleic acid structure (SNA). The orientation of the nucleic acid scaffolds played a crucial role in determining the spatial arrangement of the attached Cas9 protein, ensuring specific binding of the protein to the loop region of the extended sgRNA and the formation of a monolayer protein corona structure on the nanoparticle surface (Fig. S1).

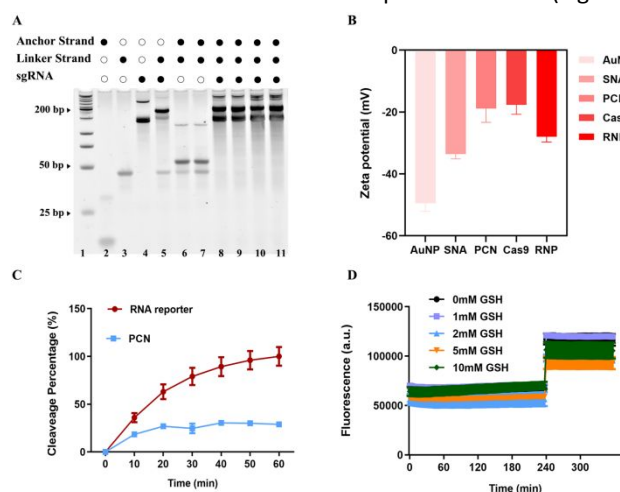


**Fig. 1** Characterization and stability assessment of AuNPs, SNAs, and PCNs. **(A)** Polyacrylamide gel electrophoresis (PAGE) analysis of annealed products formed from Anchor, Cy5-Linker, and sgRNA at varying molar ratios. Lanes: 1, marker; 2, Anchor; 3, Linker; 4, sgRNA; 5–7, sgRNA:Linker (1:1, 1:1.2, 1:1.5); 8–11, Anchor:Linker:sgRNA (1:1.2:3, 1:1.5:3, 1:1.2:5, 1:1.5:5). **(B)** Zeta potential measurements of AuNPs, SNA, PCN, free Cas9 protein, and RNP (Cas9-sgRNA complex). Stability comparison of PCN and control RNA reporters in 0.1% FBS **(C)**, and under different concentrations of glutathione (GSH) **(D)**.

Optimizing the annealing ratios of the nucleic acid strands on the gold nanoparticle surface was pivotal in achieving successful synthesis of the protein coronas. To enhance the attachment of the "anchor:linker:sgRNA" ternary complexes to the AuNPs, an excess of linker strands was essential to ensure complete pairing with all anchor strands, along with an excess of sgRNA to enable full hybridization with the anchor:linker duplex. By annealing the three strands in varying ratios, the optimal synthesis conditions were determined. Polyacrylamide gel electrophoresis (PAGE) analysis revealed that at an annealing ratio of anchor to linker of 1:1.2, complete hybridization occurred, leading to the disappearance of the anchor and linker bands. Similarly, at an annealing ratio of anchor:linker:sgRNA of 1:1.2:3, the desired three-strand complex band emerged,

indicating successful synthesis, while excess sgRNA bands were also observed (Fig. 1A).

DOI: 10.1039/D5CC03658E

The average nucleic acid scaffold loading on AuNPs was quantified using a fluorescence-based assay. Cy5-labeled Linker strands were annealed with Anchor and sgRNA at optimized ratios and anchored to AuNPs via Au-S bonds. Treatment with 2-mercaptoethanol disrupted Au-S bonds, releasing scaffolds and restoring Cy5 fluorescence. Comparing fluorescence intensities before and after release with a Cy5-DNA standard curve (Fig. S2) revealed an average loading of ~54 scaffolds per AuNP. The quantification of Cas9 protein in gel electrophoresis indicated a 64% Cas9 loading efficiency on AuNPs at a 1:100 of AuNP: Cas9 molar ratio. (Fig. S3).

Successful formation of the PCN was confirmed by characterization in UV-Vis spectroscopy. It showed red-shifted absorption peaks for PCN by 5 nm vs. AuNPs and 3 nm vs. SNAs (Fig. S4A). DLS indicated a progressive increase in hydrodynamic diameter from 32.7 nm (AuNP) to 105.7 nm (SNA) to 164.2 nm (PCN) (Fig. S4B). Zeta potential measurements further supported conjugation, increasing from citrate-stabilized AuNPs to SNAs, and rising significantly for PCN (Fig. 1B). Furthermore, the TEM results show that the nucleic acid scaffolds and Cas9 have been successfully conjugated to the AuNPs, and the synthesized PCNs exhibit superior dispersion compared to AuNPs (Fig. S5).

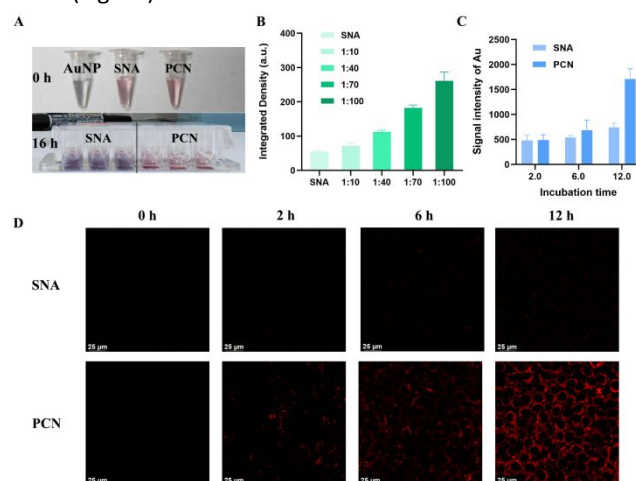


**Fig. 2** Time-dependent cellular uptake of SNA and PCN in HeLa-GFP cells. **(A)** Visual assessment of colloidal stability in cell medium: Solution state immediately after adding 1 nM AuNPs, SNA, or PCN, and solution state after 16 h incubation in cell culture wells. **(B)** Quantitative analysis of intracellular Cy5 fluorescence intensity in HeLa-GFP cells after 6 h incubation with PCNs assembled at different Cas9:SNA incubation ratios. **(C)** Intracellular Au concentration quantified by ICP-MS following incubation of HeLa-GFP cells with 1 nM SNA or PCN for 2, 6, and 12 h. Error bars represent  $\pm 1$  SD ( $n=3$ ). **(D)** Confocal fluorescence images of HeLa-GFP cells incubated with Cy5-labeled SNA or PCN for 0, 2, 6, and 12 h (Cy5 signal: red). Scale bar: 25  $\mu$ m.

The PCN significantly improved AuNP stability in complex biological systems. In 0.1% FBS, an RNA reporter was degraded completely within 40 minutes, while RNA in PCN remained stable with less than 20% degradation (Fig. 1C). PCN also demonstrated prolonged stability against glutathione (GSH), and fluorescence restoration (indicating degradation/release) occurred only upon adding 2-mercaptoethanol (2-ME) to cleave Au-S bonds, not from GSH exposure alone (Fig. 1D).





PCN also conferred superior colloidal stability in serum-free culture medium. Unmodified AuNPs aggregated immediately (solution turned gray), while both SNA and PCN initially remained dispersed (light pink). After 16 hours, SNA-treated wells showed gray aggregates, whereas PCN maintained dispersion and a pink color (Fig. 2A), demonstrating essential stability for cellular delivery applications.

We then optimized the Cas9 to SNA incubation ratio to maximize cellular uptake efficiency. Cy5-labeled SNAs incubated with increasing Cas9 ratios formed PCNs with varying protein density (Fig. S6). Co-culture with HeLa-GFP cells showed that higher Cas9 ratios progressively increased intracellular Cy5 signal (Fig. 2B), indicating enhanced transmembrane delivery. While all PCN ratios outperformed SNA, a Cas9 to SNA molar ratio of 100:1 was selected for subsequent studies to balance uptake efficiency with preventing aggregation.

While nonspecifically adsorbed proteins (e.g., serum albumin) typically reduce nanoparticle-cell membrane interactions and hinder uptake efficiency<sup>18</sup>, our designed Cas9 protein corona nanostructure demonstrates an opposite effect. The Cas9 protein's positively charged residues neutralize the negatively charged nucleic acid-modified surface, while its functional nature may facilitate receptor targeting, both mechanisms promoting cellular internalization<sup>19, 20</sup>. Furthermore, the monolayer corona's spatial arrangement potentially alters endocytic pathways<sup>21</sup>, collectively enhancing uptake.

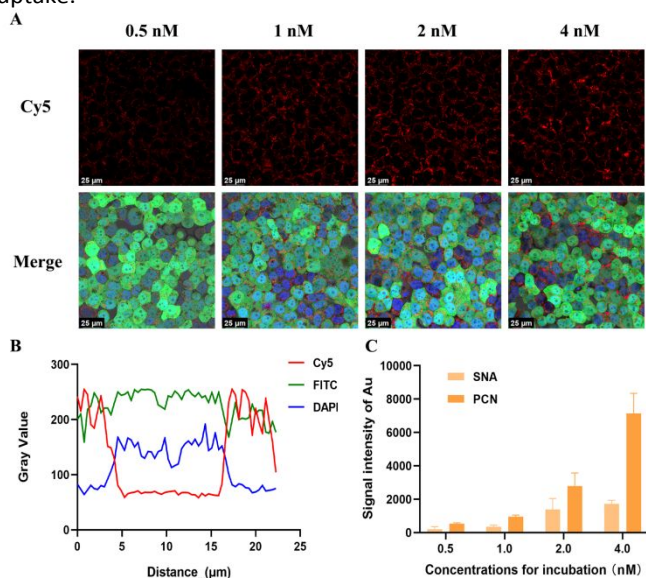


**Fig. 3** Evaluation of SNA and PCN uptake in HeLa-GFP cells at varying concentrations. **(A)** Confocal images of PCN internalization (0.5–4 nM) (Cy5, red), cells (FITC, green), nuclei (DAPI, blue). Scale bar: 25 μm. **(B)** Schematic of co-localization fluorescence analysis for a single representative HeLa-GFP cell. **(C)** ICP-MS measurement of intracellular Au after 16 h incubation with varying SNA and PCN concentrations. Error bars:  $\pm 1$  SD ( $n=3$ ).

Quantitative ICP-MS analysis of intracellular Au concentration revealed time-dependent internalization differences between SNA and PCN (Fig. 2C). After 2 hours of incubation with HeLa-GFP cells, both systems showed comparable uptake. However, prolonged incubation (6–12 h) resulted in only marginal SNA internalization increases, whereas PCN uptake surged significantly. By 12 hours, intracellular Au concentration from PCN was 2.3-fold higher than from SNA.

Fluorescence imaging of Cy5-labeled constructs corroborated with the ICP-MS results (Fig. S7). SNA showed minimal signal increase over 12 h, while PCN exhibited a gradual, time-dependent rise in intracellular Cy5 signal (Fig. 2D), confirming sustained and enhanced PCN delivery.

We further investigated the uptake efficiency of PCN with increased concentrations. Confocal imaging of HeLa-GFP cells incubated 16 h with increasing concentrations (0.5–4 nM) of Cy5-labeled PCN showed progressively stronger intracellular Cy5 fluorescence (Fig. 3A, Fig. S8). Fluorescence colocalization analysis confirmed cytoplasmic localization: Cy5 signal (PCN) overlapped extensively with cytoplasmic FITC signal but remained distinct from nuclear DAPI staining (Fig. 3B). This demonstrates successful cytoplasmic internalization without nuclear entry.

ICP-MS quantification is aligned with imaging results. The higher incubation concentrations increased intracellular Au for both SNA and PCN. Crucially, at 4 nM, PCN uptake was 4-fold greater than SNA (Fig. 3C). This significant enhancement, combined with the corona's excellent biocompatibility, suggests the Cas9 protein corona actively promotes nanoparticle-membrane interactions<sup>22</sup>, surpassing the caveolin-mediated endocytosis typical of SNAs<sup>23</sup>.

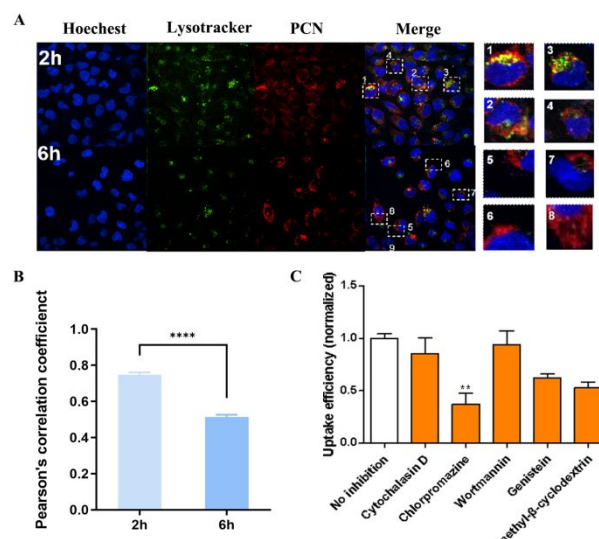


**Fig. 4** Mechanism of PCN cellular uptake and lysosomal escape. **(A)** Representative confocal images showing PCN localization relative to lysosomes and nuclei: DAPI (blue, nuclei), Cy5 (red, PCN), LysoTracker Yellow HCK-123 (green, lysosomes). **(B)** Lysosome-PCN co-localization analysis: Pearson correlation coefficient values at 2 h and 6 h incubation. **(C)** Effect of endocytosis inhibitors on PCN internalization efficiency, measured via ICP-MS.

We tracked the intracellular fate of Cy5-labeled PCN, specifically their interaction with lysosomes. Confocal fluorescence imaging after 2 hours of incubation revealed strong colocalization (Pearson's coefficient = 0.7) between PCN (Cy5, red) and lysosomes (LysoTracker Yellow, green), indicating initial lysosomal capture (Fig. 4A). However, by 6 hours, the colocalization significantly diminished (Pearson's coefficient = 0.5), demonstrating that PCN gradually escape lysosomal entrapment and achieve cytoplasmic redistribution (Fig. 4B).

To further elucidate the cellular uptake mechanism of PCN, we employed specific endocytosis inhibitors targeting distinct



pathways: cytochalasin D (phagocytosis), chlorpromazine (clathrin-mediated), wortmannin (receptor-mediated), genistein, and methyl  $\beta$ -cyclodextrin (caveolae-mediated)<sup>24</sup>. ICP-MS quantification of intracellular Au after 8 hours of incubation revealed significant pathway dependence. Chlorpromazine treatment severely impaired uptake, resulting in intracellular Au concentrations substantially lower than the inhibitor-free control. Uptake was also significantly reduced (~50% of control) by the caveolae inhibitors methyl  $\beta$ -cyclodextrin and genistein. In contrast, cytochalasin D and wortmannin had no significant effect on internalization efficiency (Fig. 4C). These results indicate that PCN primarily enter cells via clathrin-mediated endocytosis, with caveolae-mediated endocytosis playing a substantial auxiliary role.

In summary, we successfully engineered uniformly monolayer protein corona around AuNP through nucleic acid-protein assembling. This strategy achieves precise spatial arrangement of proteins on the nanoparticle surface, significantly enhancing both cellular uptake efficiency and biological stability while preserving the inherent optical properties and nanoscale functionality of the gold core. These advances substantially expand the biomedical utility of PCN for applications including drug delivery, photothermal therapy, contrast imaging, and biosensing<sup>25–29</sup>. Future exploration will focus on exploiting the Cas9-sgRNA complex for targeted gene editing delivery and extending this versatile platform to incorporate diverse nucleic acid aptamer-functional protein pairs, broadening its combinatorial potential and therapeutic scope.

H. P. thanks the financial support from the National Key Research and Development Program of China (2023YFA0915102), the Strategic Priority Research Program of the Chinese Academy of Sciences (XDB0750100) and the National Natural Science Foundation of China (Grant no. 22276199). R. S. thanks the Youth Fund from National Natural Science Foundation of China (Grant no. 22206201) for the financial support.

## Conflicts of interest

There are no conflicts to declare.

## Data availability

The data supporting this article has been included in the ESI.<sup>†</sup>

## Acknowledgement

We acknowledge the financial support from the National Key Research and Development Program of China (Grant no. 2023YFA0915102), the National Natural Science Foundation of China (Grant no. 22276199) and the Strategic Priority Research Program of the Chinese Academy of Sciences (Grant No. XDB0750100). Wenjing Xie was supported by the Youth Fund from National Natural Science Foundation of China (Grant no. 22306195).

## Notes and references

- 1 L. Dykman and N. Khlebtsov, *Chem. Soc. Rev.*, 2012, **41**, 2256–2282.
- 2 A. Albanese, P. S. Tang and W. C. W. Chan, *Annu. Rev. Biomed. Eng.*, 2012, **14**, 1–16. DOI: 10.1039/D5CC03658E
- 3 Y. Pan, S. Neuss, A. Leifert, M. Fischler, F. Wen, U. Simon, G. Schmid, W. Brandau and W. Jahnke-Dechent, *Small*, 2007, **3**, 1941–1949.
- 4 Z. Ye, W. Liao, Z. Deng, L. Wang, B. Wen, D. Zhang, H. Wang, W. Xie and H. Peng, *Trac-Trends Anal. Chem.*, 2024, **175**.
- 5 D. R. Bhumkar, H. M. Joshi, M. Sastry and V. B. Pokharkar, *Pharm. Res.*, 2007, **24**, 1415–1426.
- 6 M. Tebbe, C. Kuttner, M. Maennel, A. Fery and M. Chanana, *ACS Appl. Mater. Interfaces*, 2015, **7**, 5984–5991.
- 7 A. Anaki, C. Tzror-Azankot, M. Motiei, T. Sadan and R. Popovtzer, *Nanoscale Adv.*, 2024, **6**, 5420–5429.
- 8 C. H. J. Choi, C. A. Alabi, P. Webster and M. E. Davis, *Proc. Natl. Acad. Sci. U. S. A.*, 2010, **107**, 1235–1240.
- 9 T. Y. Chen, M. R. Chen, S. W. Liu, J. Y. Lin, Y. T. Yang, H. Y. Huang, J. K. Chen, C. S. Yang and K. M. C. Lin, *Int. J. Mol. Sci.*, 2020, **21**, 8158.
- 10 K. Knop, R. Hoogenboom, D. Fischer and U. S. Schubert, *Angew. Chem. Int. Edit.*, 2010, **49**, 6288–6308.
- 11 T. Cedervall, I. Lynch, S. Lindman, T. Berggard, E. Thulin, H. Nilsson, K. A. Dawson and S. Linse, *Proc. Natl. Acad. Sci. U. S. A.*, 2007, **104**, 2050–2055.
- 12 C. D. Walkey, J. B. Olsen, H. Guo, A. Emili and W. C. W. Chan, *J. Am. Chem. Soc.*, 2012, **134**, 2139–2147.
- 13 M. P. Monopoli, D. Walczyk, A. Campbell, G. Elia, I. Lynch, F. B. Bombelli and K. A. Dawson, *J. Am. Chem. Soc.*, 2011, **133**, 2525–2534.
- 14 M. Barz, W. J. Parak and R. Zentel, *Adv. Sci.*, 2024, **11**, 2198–3844.
- 15 J. C. Y. Kah, J. Chen, A. Zubieta and K. Hamad-Schifferli, *ACS Nano*, 2012, **6**, 6730–6740.
- 16 T. Zhao, M. Ren, J. Shi, H. Wang, J. Bai, W. Du and B. Xiang, *Biomed. Pharmacother.*, 2024, **175**.
- 17 H. Nishimasu, F. A. Ran, P. D. Hsu, S. Konermann, S. I. Shehata, N. Dohmae, R. Ishitani, F. Zhang and O. Nureki, *Cell*, 2014, **156**, 935–949.
- 18 W. Kim, N. K. Ly, Y. He, Y. Li, Z. Yuan and Y. Yeo, *Adv. Drug Deliv. Rev.*, 2023, **192**, 1872–8294.
- 19 R. Cai and C. Chen, *Adv. Mater.*, 2019, **31**, 1521–4095.
- 20 M. Barbalinardo, F. Caicci, M. Cavallini and D. Gentili, *Small*, 2018, **14**, 1613–6829.
- 21 X. Cheng, X. Tian, A. Wu, J. Li, J. Tian, Y. Chong, Z. Chai, Y. Zhao, C. Chen and C. Ge, *ACS Appl. Mater. Interfaces*, 2015, **7**, 20568–20575.
- 22 J. Wu, H. Peng, X. Lu, M. Lai, H. Zhang and X. C. Le, *Angew. Chem. Int. Edit.*, 2021, **60**, 11104–11109.
- 23 A. Mokhtarzadeh, H. Vahidnezhad, L. Youssefian, J. Mosafer, B. Baradaran and J. Uitto, *Trends Mol. Med.*, 2019, **25**, 1066–1079.
- 24 V. Francia, K. Yang, S. Deville, C. Reker-Smit, I. Nelissen and A. Salvati, *ACS Nano*, 2019, **13**, 11107–11121.
- 25 A. Yuan, T. Sun, L. Chen, D. Zhang, W. Xie and H. Peng, *Anal. Chem.*, 2024, **96**, 20074–20081.
- 26 A. Yuan, R. Sha, W. Xie, G. Qu, H. Zhang, H. Wang, X. C. Le, G. Jiang and H. Peng, *J. Am. Chem. Soc.*, 2024, **146**, 26657–26666.
- 27 R. Sha, H. Qin, A. Yuan, Z. Deng, W. Liao, G. Qu, B. Wen, W. Xie and H. Peng, *Chem. Asian J.*, 2025, 1861–4728.
- 28 Q. Liu, Y. Ouyang, Y. Wang, S. Zhou, Y. Zhan, L. Wang, *Adv. Healthc. Mater.*, 2025, 2405058.
- 29 L. Wang, S. Zhou, Y. Wang, Y. Wang, J. Li, X. Chen, D. Zhou, L. Liang, B. Yin, Y. Zhang, L. Wang, *Faraday Discuss.*, 2025, **257**, 60–72.

<sup>†</sup> Electronic supplementary information (ESI) available. See DOI:

<sup>‡</sup> These authors contributed equally.



**Data Availability Statement**

The data supporting this article has been included in the ESI.

Open Access Article. Published on 21 August 2025. Downloaded on 8/28/2025 1:59:58 PM.  
This article is licensed under a Creative Commons Attribution-NonCommercial 3.0 Unported Licence.

